Atmospheric washout of ^{35}S during single rain events – implications for ^{35}S sampling schemes

M. Schubert[1], S. M. Weise[2], K. Knöller[2]

[1] *UFZ Helmholtz Centre for Environmental Research, Permoserstr. 15, 04318 Leipzig, Germany*

[2] *UFZ Helmholtz Centre for Environmental Research, Theodor-Lieser-Str. 4, 06120 Halle, Germany*

ABSTRACT: Cosmogenic radiosulfur (^{35}S; half-life: 87.4 days) is transferred with the rain to the groundwater (as ^{35}SO$_4^{2-}$) and can be used as residence time tracer for the detection of sub-yearly groundwater residence times. Due to the distinct but non-regular annual ^{35}S pattern in precipitation, related data evaluation requires consideration of a ^{35}S input function that is based on representative rain samples. While minor rain events can easily be sampled quantitatively and hence representatively, a long-lasting rain event may get documented by a sample that represents only a certain sequence of the event, thus potentially resulting in a ^{35}S activity concentration that might not be representative. With the aim to examine the magnitude of temporal variations of the ^{35}S activity concentration in rain during long-lasting rain events, we present and discuss two related exemplary ^{35}S time series. Furthermore, we evaluate the applicability of the parameters total sulfate and electrical conductivity (EC), both detected in rainwater as easily attainable ^{35}S proxies. The results of the study show (i) that the ^{35}S activity concentration may vary substantially during long-lasting rain events due to atmospheric migration processes and aerosol washout and (ii) that neither sulfate nor EC are suitable as ^{35}S proxies due to the different origin of ^{35}S on the one hand and sulfate/EC on the other. Hence, for the determination of a ^{35}S activity concentration that is representative for a long-lasting rain event ^{35}S analyses of an adequate number of sub-samples cannot be avoided.

Keywords: ^{35}S; input function; short term variation; groundwater residence time; tracer

1 Introduction

The knowledge of groundwater residence times is essential for (i) assessing the vulnerability of aquifers, (ii) ensuring sustainable groundwater abstraction management and (iii) evaluating groundwater migration patterns and associated dissolved matter fluxes. Environmental radio-tracers, i.e., radionuclides that occur naturally in rain and hence groundwater, are known as a powerful toolset for related investigations.

While some of the radionuclides that are commonly used as aqueous tracers occur with an almost time-constant activity concentration in the atmosphere and hence in the rain that is recharging the groundwater (e.g., ^{39}Ar; Loosli, 1983), others show distinct temporal patterns. For application of the latter as groundwater dating tools, nuclide-specific input functions for the recharged aquifer are required. A well-known example for these time-variant tracers is tritium (^{3}H; half-live: $t_{1/2}$ = 12.3 years; Lucas & Unterweger, 2000). Its groundwater input function, which results mainly from the numerous atmospheric nuclear bomb tests executed around the early 1960s, is well defined for most areas worldwide. In contrast, setting up an input function for a radio-tracer that is added to the atmosphere continuously at varying rate (e.g., ^{85}Kr; $t_{1/2}$ = 10.8 years; Kersting et al., 2020) is more challenging.

Since studies of groundwater recharge and contamination concern generally shallow aquifers, groundwater residence times between only a few months and one year are in many cases of major interest. Among the (few) short-lived radioisotopes that can be used as dating tracers for this time range is a naturally occurring radioactive isotope of sulfur, namely ^{35}S ("radiosulfur", $t_{1/2}$ = 87.4 days). ^{35}S has only recently been introduced to the scientific community as an environmental radio-tracer suitable for covering sub-yearly groundwater residence times (Lin & Thiemens, 2018; Urióstegui et al., 2015; Urióstegui et al., 2016).

Radiosulfur is continuously produced by cosmic ray spallation (of ^{40}Ar) in the stratosphere where it instantly oxidizes to sulfate. Due to its short half-life, some of the produced ^{35}S decays to ^{35}Cl right in the stratosphere and troposphere. Still, most of it gets dissolved in the meteoric water as ^{35}SO$_4^{2-}$ and is transferred with the precipitation to the Earth's surface and finally to the groundwater (Tanaka & Turekian, 1991).

^{35}S activity concentrations in rain range roughly between about 10 and 150 mBq/L (Urióstegui et al., 2016; Cho et al., 2011; Hong & Kim, 2005; Osaki et al., 1999). As soon as the ^{35}S containing meteoric water enters the subsurface, ^{35}S decay is not compensated by atmospheric ^{35}S production anymore, which makes the decline of the ^{35}S activity concentration in the groundwater an indicator for its

32 residence time in the subsurface determined by the ^{35}S decay constant. This makes radiosulfur a

33 residence time tracer suitable for groundwater ages between about three and nine months (i.e.,

34 between about one and three ^{35}S half-lives; Michel et al., 2000; Sueker et al., 1999; Visser et al.,

35 2019).

36 The so far published practical case studies that used ^{35}S as residence time tracer are discussing

37 groundwater recharge in high geographical elevations, where the snowmelt is the dominant recharge

38 event. That limits the ^{35}S input to a temporarily narrow event and simplifies the related input function

39 to a distinct value (Michel et al., 2000; Sueker et al., 1999; Shanley et al., 2005; Cooper et al., 1991).

40 However, if ^{35}S studies are carried out in more moderate climate zones where precipitation, as

41 sole ^{35}S source to the groundwater, occurs more or less continuously throughout the year, it has to

42 be taken into account that ^{35}S in rain shows a substantial variability over the course of a year (e.g.,

43 Schubert et al., 2020a; Plummer et al, 2001; Turekian & Tanaka, 1992). This varying ^{35}S input value

44 is mainly due to large-scale atmospheric circulation dynamics, i.e., due to stratosphere / troposphere

45 air mass exchange and convective tropospheric air circulation, which are, to a large degree, bound

46 to seasonal patterns in large-scale atmospheric processes and result generally in lower ^{35}S values

47 during the cold season (Schubert et al., 2020a).

48 If ^{35}S is to be used as short-term residence time tracer in groundwater studies, the distinct annual

49 variation of ^{35}S in rain necessitates setting up a ^{35}S input function, which should cover at least

50 three ^{35}S half-lives (i.e., about nine months) previous to the groundwater sampling campaign. Setting

51 up such input function requires collecting and analyzing samples of an appropriate number of rain

52 events during this period. Since in particular long-lasting moderate rains are likely to have significant

53 impact on groundwater recharge and hence on both groundwater composition and ^{35}S input function

54 they have to be sampled with particular caution. At the same time, long-lasting rain events are often

55 a result of large-scale atmospheric patterns that are potentially characterized by significant temporal

56 changes in origin and composition of both air mass and water vapor during the rain event. That in

57 turn may result in a significant temporal change in rain composition, i.e., might be a source of error

58 for the result if the rainfall dynamics (i.e., the washout of the atmospheric sulfate by precipitation) are

59 not being taken into account for data evaluation (Taylor et al., 2016; Chae & Kim, 2019).

60 In order to shed light on the variability of ^{35}S in rain during long-lasting rain events, we investigated ^{35}S

61 variations in precipitation recorded during two exemplary rain events and analyzed the resulting

62 implications for related sampling schemes. Since ^{35}S analysis is rather laborious (Schubert et al.,

63 2019; Schubert et al., 2020b) we did furthermore evaluate the applicability of three easily attainable

64 parameters all detected in rainwater, namely total sulfate and electrical conductivity as ^{35}S proxies

65 potentially applicable for studying $^{35}SO_4^{2-}$ washout dynamics during long-lasting rain events.

66

67 2 Materials and methods

68 2.1 Sampling and measurement

69 A rain sampling station was installed, uncovered by trees, in a rural environment close to the City of

70 Leipzig, Germany. The area is located at an elevation of 155 masl, characterized by an average

71 annual rainfall of 550 mm and an average annual temperature of 11°C. During the two investigated

72 rain events all samples were collected from a 31 m² inclined laminated rain collector plane via a

73 downpipe into a 0.2 m³ HDPE container. The container was protected from any other environmental

74 depositions besides rain. The rain collector surface, the downpipe and the container had been

75 cleaned prior to both rain events.

76 All required associated meteorological data was recorded at the sampling site and, as backup,

77 at a professional meteorological station located only 3 km away (on the far side of a major river,

78 though).

79 Each rain sample was representatively transferred from the HDPE container into a 20-litre plastic

80 canister. Since no elevated sulfate concentrations had to be expected in the samples (Schubert et

81 al., 2019), all sample processing for ^{35}S measurement followed the suggestions for low-sulfate sample

82 preparation for Liquid Scintillation Counting (LSC) given by Schubert et al. (2020b). A Quantulus GCT

83 6220 liquid scintillation counter was used for all ^{35}S measurements. For allowing reasonable statistical

84 reliability of the counting results (counting error < 5 %), each LSC measurement lasted 24 hours. The

85 detection background (about 7 cpm) was counted and subtracted from the sample counts by

86 measuring a ^{35}S-dead (and ^{3}H-dead) background vial before each measurement.

87 Prior to sample processing for ^{35}S measurement aliquots of the samples were taken and used for

88 stable isotope analyses of hydrogen and oxygen (δ^2H, δ^{18}O; "D/O"). The D/O measurements (always

89 doublets from two batches) were carried out using laser cavity ring-down spectroscopy (Picarro

90 L2120-i, Santa Clara, USA). The results are expressed as delta notations relative to the Vienna

91 Standard Mean Ocean Water (VSMOW). The analytical uncertainties (1σ) of δ^2H and of δ^{18}O

92 measurements are ±0.8 ‰ and ±0.2 ‰, respectively.

Furthermore, aliquots of the samples were taken for total sulfate analysis. Sulfate concentrations in water were analyzed after 0.45 micron filtration by ion chromatography using a Dionex ICS-2000 combined with AS50. Electrical conductivity (EC) was measured using a multi-parameter probe (WTW Germany).

2.2 Investigated rain events

All rain samples were taken in fall and winter 2020 during two sampling campaigns both characterized by long-lasting rain events. While all event specific meteorological data was recorded at the sampling site and at a nearby meteorological station (as described above), information about the actual macro weather situations was obtained from the open source database of the German Weather Service - DWD (in German; www.dwd.de/DE/leistungen/grosswetterlage/grosswetterlage.html).

The first event (i.e., the first sampling campaign) lasted for 52 hours from Oct. 14th 2020, 01:00 a.m. until Oct. 16th 2020, 07:00 a.m. with continuing rainfall totaling 44.5 mm. The majority of the rain (35.8 mm) fell throughout the first 19 hours of the event (Figs. 1 and 2). The individual samples were taken every two hours during the initial intense rain (samples #1 - #5) and every three hours during the following period of lessening but still intense rain (samples #6 - #8). The samples #9 - #11 were taken as soon as a cumulative amount of rain had been collected, that made a new sample reasonable in the given context.

The rain event resulted from a large-scale low pressure system that had built up in northern Italy in the night 11th/12th October. While increasing in intensity the weather system had traversed on an anti-clockwise path over the northern Balkan and western Hungary to end up in south-eastern Poland. From there it changed its path on the evening of Oct. 13th and started moving straight westward to settle finally in south Poland in the early hours of Oct. 14th. There the system stabilized as anti-clockwise low pressure cyclone and sent a continuous and long-lasting stream of very moist and (for the season) warm air to eastern Germany (Fig. 1). There this warm moist air mass slid over a cold air layer that was covering Germany at the time. This resulted in the continuous formation of heavy Nimbostratus clouds, which reached very high elevations and triggered continuous rain particularly over eastern and central Germany.

The second rain event (i.e., the second sampling campaign) lasted for five days from Dec. 21st until Dec. 25th 2020, however with lighter and discontinuous rainfall. The rain summed up to a total amount

123 of 13.6 mm. Due to the minor intensity of the rainfall the individual samples were taken as 24 hours

124 composite samples, i.e., as representative for each day of the event.

125 The onset of this long-lasting event was due to a large-scale cyclonic system that had settled over

126 Germany bringing in large masses of moist air and significant amounts of rain from the central Atlantic

127 Ocean. This continuous large-scale airstream from the west changed its direction in the progression

128 of the event. In the night Dec. 21st/22nd the airstream from the west was replaced by a stream of

129 significantly warmer air masses coming from the southwest, a pattern that reached its peak on

130 Dec. 22nd with (for the season) unusually high temperatures of over 10°C. The end of this warm period

131 was accompanied by the highest rain intensities of the overall rain event on Dec. 23rd. Finally on

132 Dec. 24th the direction of the airstream changed again, now suddenly bringing in arctic polar air from

133 the north (Fig. 1). The rain activity finally ceased with this cold snap.

134
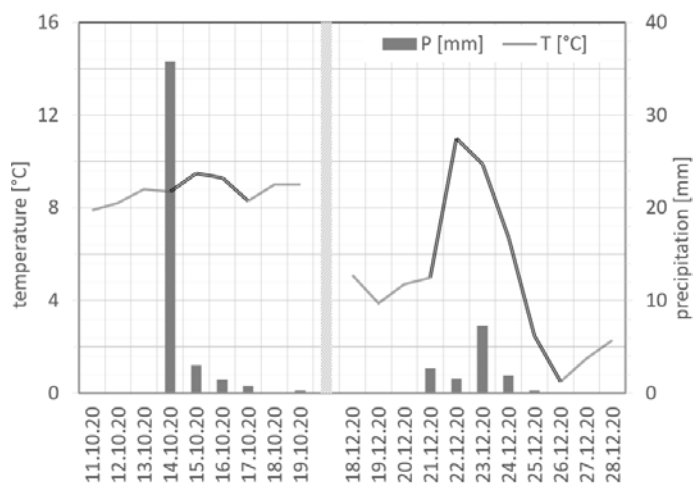
135

136 Fig. 1: Daily average precipitation (P) and air temperatures (T) during the two investigated rain events.

137 The bold lined sections in the temperature plots illustrate the periods of monitoring

138

139 3   Results

140 3.1 The first rain event

141 During the continuous 52 hours rain event a total number of eleven sets of rain samples were taken

142 (#1 - #11). Each set comprised three samples, one for ^{35}S (20 liters), one for D/O (100 ml) and one

143 for sulfate (100 ml). Each of the individual samples is representative for the rain that fell in the time

144 period between the actual sampling and the previous one. The first set of samples (#1) is

145 representative for the initial 1.6 mm of rain that fell during the first two hours of the rain event (Oct. 14th

146 2020, 01:00 a.m. – 03:00 a.m.).

147   As displayed in Fig. 2, the precipitation intensity increased more or less continuously until a peak was

148   reached after about eleven hours of rainfall (sample #6). Subsequently the rain intensity lessened

149   until it steadied at a rate of about 0.3 mm/h after another eight hours (sample #9; total time count 19

150   hours). Afterwards the rain continued with a very low (and still declining) intensity until it ceased

151   completely after 52 hours of continuous rainfall (sample #11).

152
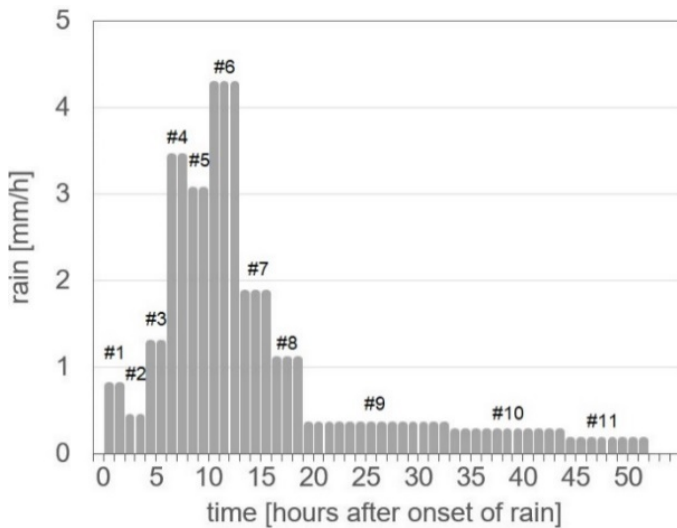
153

154   Fig. 2: Average hourly rain intensity recorded (and sampled) in eleven steps during the first rain event

155

156   The EC of the rain was used as a preliminary and easily attainable indicator for the time variant

157   intensity of aerosol washout by the rain. The resulting dataset is displayed in Fig. 3. The data shows

158   a drop in EC to about a third of its onset value within the first twelve hours of rain, i.e., until the peak

159   in rain intensity was reached (sample #6). During this period of decreasing EC the parameter showed

160   only a short (and marginal) recovery after about eight hours (sample #5).

161   Following the intense rain period, which ended after about 19 hours (samples #1 - #8), the EC started

162   to rise again continuously with a gradient that was increasing with time. The rain sample that

163   represents the last eight hours of (at the time) very light rain (#11) showed even an EC value that was

164   about 15 % above the value detected at the beginning of the rain event (11.6 µS/cm and 10.0 µS/cm,

165   respectively).

166   Overall the recorded EC time series points toward an intense aerosol washout until the rainfall peak,

167   which is followed by a recovery of the atmospheric density of aerosols. The latter is most likely due

168   to both an arrival of "fresh" aerosol laden air masses drifting in from the east and a simultaneous

169   significant decrease in rainfall intensity.
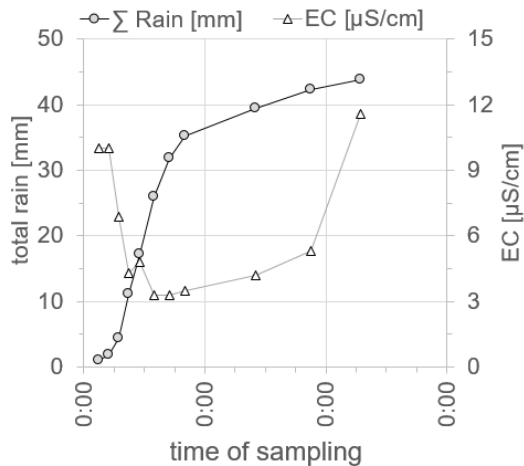
170

171 Fig. 3: Cumulative rain during the first rain event summing up to 44 mm and electrical conductivity

172 (EC) in the eleven samples taken

173

174 Fig. 4A displays the time series of the total sulfate concentration in rain and the ^{35}S activity that is

175 contained in this sulfate. ^{35}S plots close to sulfate with both parameters showing significantly higher

176 values at the end of the rain event compared to its start (^{35}S: 38.9 mBq/L and 15.6 mBq/L,

177 respectively). This similar behavior of dissolved sulfate and ^{35}S reflects also in a determination

178 coefficient of R^2 = 0.88 (Fig. 4B). If compared with EC (see Fig. 3) in particular the sulfate plot reveals

179 a generally analogous behavior (R^2 = 0.91; data not displayed), indicating an initial sulfate washout

180 followed by sulfate recovery for the same reasons as given for EC. It can even be seen that sulfate

181 (as well as ^{35}S) shows the same short and marginal peak after about eight hours (sample set #5) that

182 was also observed for EC.
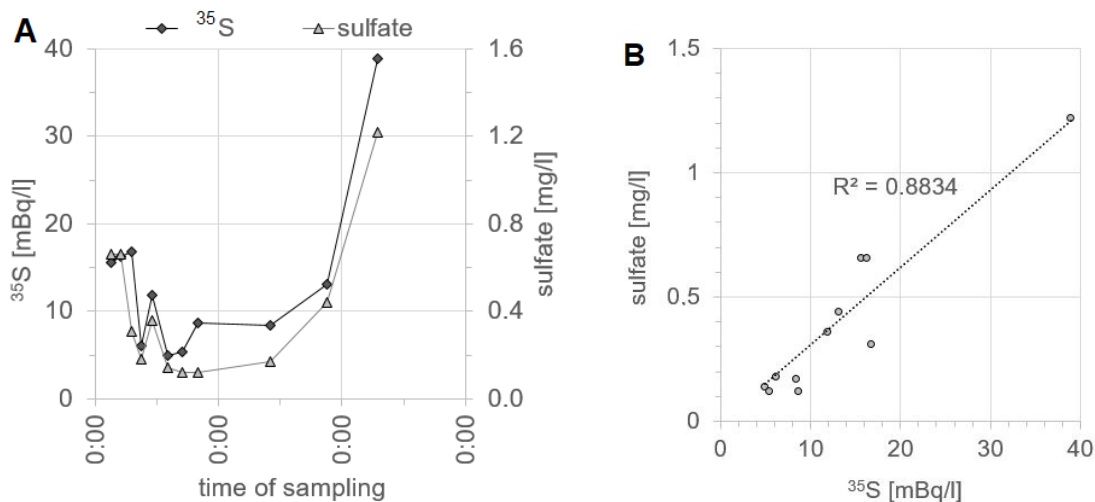
183

184 Fig. 4A: Time series of ^{35}S activity and sulfate concentration as f(t)

185 Fig. 4B: Time series of sulfate concentration vs. ^{35}S activity

186 However, in contrast to EC, sulfate reached at the end of the rain event concentrations that nearly

187 doubled the onset value (1.22 mg/L and 0.66 mg/L, respectively). ^{35}S showed a virtually analogous

188 increase with a final concentration even more than twice the initial value (38.9 mBq/L and 15.6 mBq/L,

189 respectively). Since ^{35}S originates solely from the upper atmosphere, local terrestrial

190 (e.g., anthropogenic) sources can be ruled out as ^{35}S sources. Hence it can be concluded that the

191 composition of the air masses that were drifting in as a large-scale pattern and that were washed out

192 by the rain had changed halfway through the rain event (as concluded from the EC data as well). The

193 aerosol composition of these "fresh" air masses was more dominated by total sulfate than the air that

194 was present (and washed out) at the beginning of the rain event.

195 Fig. 5 displays the time series of the isotopic composition of the rainwater recorded during the

196 52 hours rain event as revealed by the parameters $δ^2H$ and Deuterium excess (*d*). The purpose of

197 the stable isotope measurements was not directly associated to investigating the washout behaviour

198 of ^{35}S. The data was rather needed for understanding the nature of the rain event, i.e., the origin of

199 air mass and water vapour that might cause temporal changes of the ^{35}S activity concentration of the

200 rain.

201 The $δ^2H$ plot shows that in the beginning of the event (sample sets #1 – #5) deuterium got more and

202 more depleted, i.e., that the rain got depleted in heavier isotopes with ongoing and increasing rainfall.

203 This observation is consistent with isotopic trends detected in earlier studies of frontal and convective

204 precipitation events as they are typical for frontal systems surrounding low pressure cyclones, which

205 form when warm air meets cooler air as in the present situation (e.g., Dansgaard, 1964; Celle-Jeanton

206 et al., 2004; Aemisegger et al., 2015). When a cold air mass underlays a warm and humid air mass,

207 it causes its rise (typically building nimbostratus clouds) accompanied by an adiabatic cooling

208 resulting in descending isotopic trends in the precipitation (Celle-Jeanton et al., 2004). However,

209 subsequently to sample #5 (and with no temporary plateau phase) $δ^2H$ started to rise again with a

210 similar (but inverse) slope forming a V-shaped pattern. Comparable patterns have been interpreted

211 as being produced by frontal and convective precipitation events, when the later phase of the event

212 (i.e., the ascending arm of the $δ^2H$ plot) obeys an internal mechanism that is considerably different to

213 the initial phase (i.e., the descending arm) resulting in a vapor source of different quality (Celle-

214 Jeanton et al., 2004). This underpins the assumption of a significant change in composition and

215 quality of the large-scale air and hence vapor masses halfway through the rain event made based in

216 the EC, sulfate and ^{35}S data.

217　The parameter Deuterium excess (d) allows generally resolving differences between the two

218　commonly used parameters δ²H and δ¹⁸O in more detail. The typical Deuterium excess mean value

219　at the sampling station is ca. 8 ‰ (based on long-term local observations (IAEA)). All Deuterium

220　excess values in this study were calculated based on Eq. 1 (Dansgaard, 1964).

221
$$d = \delta\,^{2}H - 8 \cdot \delta^{18}O$$
Eq.1

222　As displayed in Fig. 5, all Deuterium excess values plot (with a minimum value of 12.2 ‰) significantly

223　above the ≈ 8 ‰ level that would be expected for the region. The recorded d values of up to almost

224　20 ‰ are rather typical for a Mediterranean origin of cloud vapor (Gat & Carmi, 1970). This is in

225　accordance with the fact that the causal large-scale low pressure system had built up in northern Italy

226　(as described in sect. 2.2,). Along the ascending arm of the δ²H plot (starting with sample #5) the

227　Deuterium excess follows the δ²H trend fairly closely. Only in the final period of the rain event

228　(samples #10 and #11) d drops again to a slightly lower level. Still, subsequently to sample #5 the

229　generally parallel trends of δ²H and d point to common causal processes, such as rain contribution

230　from a vapor source different in quality compared to the onset of the rain. This assumption could also

231　explain why the time series of both δ²H and δ¹⁸O (the latter not displayed in Fig. 5) end finally with

232　values that are significantly higher than the signatures observed at the beginning of the rain event

233　(comparable to sulfate and ³⁵S; Fig. 6).

234
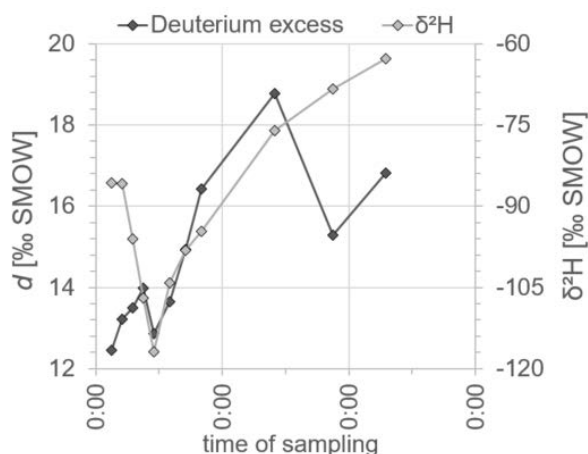
235

236　Fig. 5: Time series of δ²H and Deuterium excess (d) in the samples taken

237
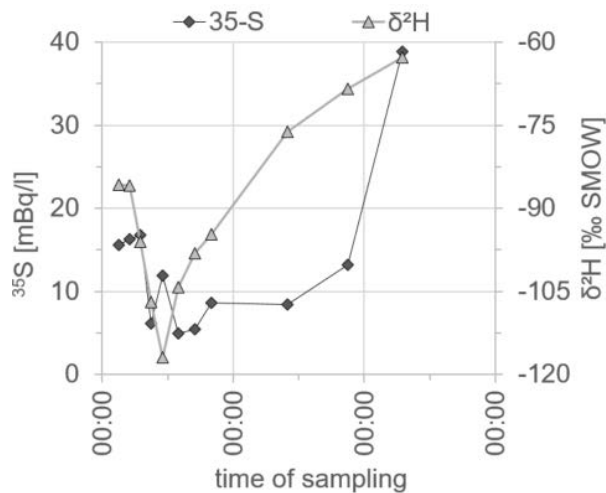
Fig. 6: Time series of ^{35}S activity and δ^2H signature in the samples taken

3.2 The second rain event

The second monitored rain event lasted for five days from Dec. 21st until Dec. 25th 2020. In contrast to the first event the rain did not fall continuously but with several interruptions, each lasting several hours, ending up with a total rain amount of 13.6 mm. Hence, only five sets of samples were taken, each one representing the cumulative rainfall of one day. This only limited number of samples and the discontinuous nature of the rainfall do not allow a data evaluation as thoroughly and statistically reliable as for the first event. Still, the observed trends can be discussed in comparison to those recorded during the first event.

As displayed in Fig. 7, the rain resulted generally in a significant washout of aerosols from the atmosphere. The ^{35}S activity concentration dropped by 66 % from 35 to 12 mBq/L. The most pronounced ^{35}S washout (with concentrations declining from 30 to 11 mBq/L) occurred during the third day of the event (Dec. 23rd; 7.3 mm), i.e., during the period of most intense rainfall. The EC of the rainwater declined also significantly throughout the five day event. Even though the plots of EC and ^{35}S differ, the washout resulted overall in a comparable decrease of the two components.
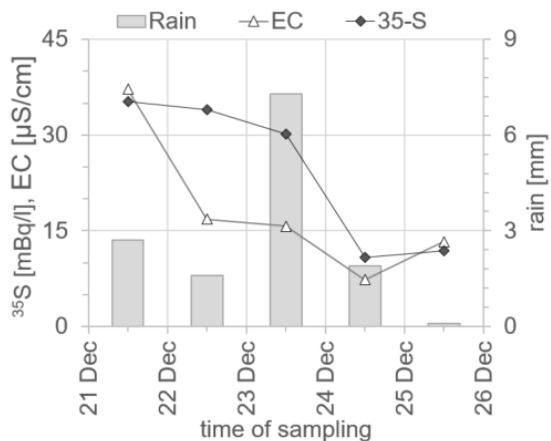
256

257 Fig. 7: Daily rainfall (summing up to 13.6 mm in total), electrical conductivity (EC) and ^{35}S in the five

258 daily samples taken during the second rain event

259

260 The intense aerosol washout reflects also in the recorded sulfate values, which dropped by 77 % from

261 5.3 to 1.3 mg/L (Fig. 8). Still, even though the washout resulted in a comparable overall decrease of

262 both sulfate and ^{35}S, the shapes of the two plots differ (as also observed for EC and ^{35}S). While the

263 most noticeable sulfate washout occurred on the first day of the rain event, the ^{35}S values decreased

264 most pronouncedly on the third day, i.e., on the day of most intense rain. The different shapes of the

265 sulfate and ^{35}S plots can be explained with the different origins of total sulfate and ^{35}S, the first

266 originating from (local) terrestrial (e.g., anthropogenic) sources and the latter from the higher

267 atmosphere. Hence, it can be stated that while the sulfate of terrestrial origin is rather continuously

268 washed out of the lower atmosphere, the ^{35}S activity concentration in rain is much more dependent

269 on the large-scale origin of the rain producing water vapor. This conclusion is supported by the fact

270 that the most pronounced change in ^{35}S on the third day coincides with the increasing impact of air

271 masses of arctic origin (*cf*. sect. 2.1).

272
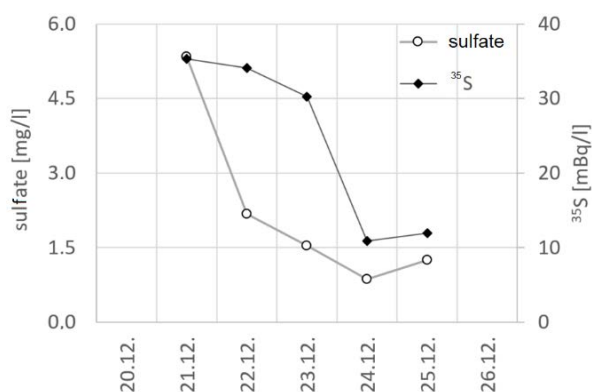
273

274 Fig. 8: Total sulfate and ^{35}S in the five daily samples taken during the second rain event

275   The varying characteristics of the incoming air stream is also confirmed by the variation of the

276   parameters δ^2H and Deuterium excess (*d*) during the second rain event (Fig. 9). Compared to the V-

277   shape of the δ^2H plot recorded during the first rain event, δ^2H shows a different (almost inverse)

278   behavior here. Coming from an initial value of -80 ‰, δ^2H peaks at -40 ‰ in the middle of the event

279   and drops subsequently with a steep gradient back to -90 ‰. A rain sample that was collected from

280   a subsequent individual rain shower (Dec. 27th, not displayed in Fig. 9) showed an even lower δ^2H

281   signature of -125 ‰. The descending arm of the δ^2H plot, i.e., the shift from isotopically "heavier" to

282   isotopically "lighter" rain during the second half of the five days period, reflects the changing origin of

283   the causing water vapor. The rain event started with water condensing from vapor coming from the

284   central Atlantic, continued with rain produced from vapor originating in more south-eastern regions

285   (still Atlantic, though, not the Mediterranean) and ended finally (after the third day) with vapor and

286   hence rainwater from a cold arctic origin.

287   The Deuterium excess values do also reflect this severe meteorological shift in the course of the rain

288   event. Starting with 8 ‰ (as being typical for the sampling area), the subsequent significantly lower *d*

289   values of 4 – 5 ‰ (Dec. 22nd – Dec. 24th) coincide with the arrival of the warmer air masses coming

290   from a more southern Atlantic region. Cause for the low *d* values might be an unusually low relative

291   humidity (< 70 %) of the air that received the evaporated sea water. In contrast, *d* values higher than

292   typical for the area (e.g., 10.4 ‰, 13.9 ‰ and 15.8 ‰ detected on Dec. 27th Jan. 3rd, and Jan. 4th

293   respectively, not displayed in Fig. 9) indicate precipitation from air masses of colder origin (Araguas-

294   Araguas et al., 2000; Merlivat & Jouzel, 1979), i.e., represent the arriving cold spell.

295

296
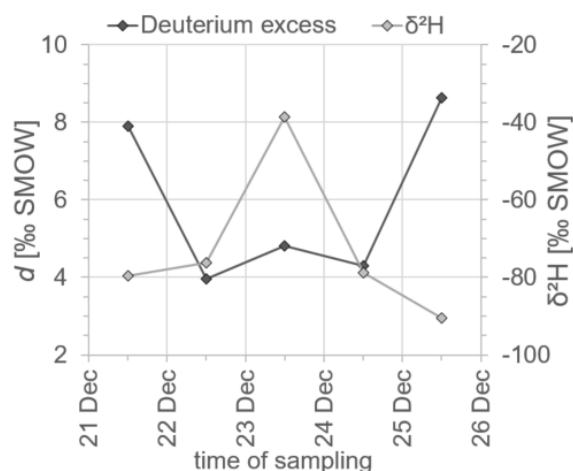
297   Fig. 9: δ^2H and Deuterium excess (*d*) in the five daily samples taken during the second rain event

298

299   Since ^{35}S analysis is rather laborious Schubert et al. (2020a) suggested using ^{7}Be in atmospheric air

300   as proxy for ^{35}S. ^{7}Be is recorded as routine atmospheric parameter by the Comprehensive Nuclear-

301   Test-Ban Treaty Organization (CTBTO) at stations worldwide and datasets are freely available.

302   However, at CTBTO stations ^{7}Be is recorded only as daily average value, which makes the data

303   inappropriate for studying short-time events such as single rainfalls. Furthermore, the distance

304   between the ^{35}S sampling location and the closest CTBO station will generally result in significant

305   differences in removal of both ^{35}S and ^{7}Be from surface air due to differences in the prevailing

306   meteorological conditions (especially differences in rainfall) at each site.

307

308   4   Conclusions

309   Using ^{35}S as short-term residence time tracer in groundwater studies requires setting up a ^{35}S input

310   function. This in turn necessitates the collection of representative rain samples over a period of about

311   nine months. In this context, long-lasting rain events have to be treated with particular care as the

312   results of our study reveal a high probability of temporal changes in the ^{35}S activity concentration of

313   the rain during such long-lasting rain events. Hence, the collection and analysis of an adequate

314   number of samples that are representing the complete event is required.

315   At the same time, the rather laborious analysis of ^{35}S in water samples makes minimizing the number

316   of ^{35}S analyses desirable. That calls for an optimized approach based on more easily attainable ^{35}S

317   proxies that are recorded simultaneously during the rain event. However, the results of our study

318   showed that the easily attainable parameters EC and sulfate cannot unrestrictedly be used as ^{35}S

319   proxies in rain due to the different origin of ^{35}S on the one hand and EC/sulfate on the other. While ^{35}S

320   is produced solely in the upper atmosphere, EC and sulfate are of terrestrial (and potentially

321   anthropogenic) origin. Changes of the individual parameters during a rain event are hence potentially

322   triggered by different causes.

323   Hence, we suggest that executing ^{35}S analysis of an adequate number of samples that are

324   representative for a long-lasting rain event cannot be avoided. An alternative option would be to take

325   a composite sample large enough to represent the complete event.

326

327

328

329

330 References

331 Aemisegger, F., Spiegel, J.K., Pfahl, S., Sodemann, H., Eugster, W., Wernli, H. 2015. Isotope

332   meteorology of cold front passages: A case study combining observations and modelling.

333   Geophysical Research Letters 42, 5652-5660.

334 Araguas-Araguas, L., Froehlich, K., Rozanski, K. 2000. Deuterium and oxygen-18 isotope

335   composition of precipitation and atmospheric moisture. Hydrological Processes 14, 1341-1355.

336 Celle-Jeanton, H., Gonfiantini, R., Travi, Y., Sol, B. 2004. Oxygen-18 variations of rainwater during

337   precipitation: application of the Rayleigh model to selected rainfalls in Southern France. Journal

338   of Hydrology 289, 165-177.

339 Chae, J., Kim, G. 2019. Large seasonal variations in fine aerosol precipitation rates revealed using

340   cosmogenic ^{7}Be as a tracer. Science of the Total Environment 673, 1-6.

341 Cho, H.-M., Hong, Y.-L., Kim, G. 2011. Atmospheric depositional fluxes of cosmogenic ^{35}S and ^{7}Be:

342   Implications for the turnover rate of sulfur through the biosphere. Atmospheric Environment 45,

343   4230-4234.

344 Cooper, L.W., Olsen, C.R., Solomon, D.K., Larsen, I.L., Cook, R.B., Grebmeier, J.M. 1991. Stable

345   isotopes of oxygen and natural and fallout radionuclides used for tracing runoff during snowmelt

346   in an Arctic watershed. Water Resources Research 27, 2171-2179.

347 Dansgaard, W. 1964. Stable isotopes in precipitation. Tellus XVI, 436-468.

348 Gat, J.R., Carmi, I. 1970. Evolution of the isotopic composition of atmospheric waters in the

349   Mediterranean Sea area. Journal of Geophysical Research 75, 3039–3048.

350 Hong, Y., Kim, G. 2005. Measurement of Cosmogenic ^{35}S Activity in Rainwater and Lake Water.

351   Analytical Chemistry 77, 3390-3393.

352 International Atomic Energy Agency – IAEA, Global Network of Isotopes in Precipitation (GNIP),

353   station Leipzig, see https://www.iaea.org/services/networks/gnip.

354 Kersting, A., Schlosser, C., Bollhöfer, A., Suckow, A. 2020. Evaluating 5 decades of atmospheric ^{85}Kr

355   measurements in the southern hemisphere to derive an input function for dating water and ice with

356   implications for interhemispheric circulation and the global ^{85}Kr emission inventory. Journal of

357   Environmental Radioactivity 225, 106451.

358 Lin, M., Thiemens, M.H. 2018. Accurate Quantification of Radiosulfur in Chemically Complex

359   Atmospheric Samples. Analytical Chemistry 90, 2884-2890.

360 Loosli, H.H. 1983. A dating method with ^{39}Ar. Earth and Planetary Science Letters 63(1), 51-62.

361 Lucas, L.L., Unterweger, M. P. 2000. Comprehensive review and critical evaluation of the half-life of
362   Tritium. Journal of Research of the National Institute of Standards and Technology 105(4), 541-
363   549.

364 Merlivat, L., Jouzel, J. 1979. Global climatic interpretation of the deuterium-oxygen-18 relationship for
365   precipitation. Journal of Geophysical Research 84, 5029-5033.

366 Michel, R.L., Campbell, D., Clow, D., Turk, J.T. 2000. Timescales for migration of atmospherically
367   derived sulphate through an alpine/subalpine watershed, Loch Vale, Colorado. Water Recourses
368   Research 36, 27-36.

369 Osaki, S., Tagawa, Y., Chijiiwa, T., Sugihara, S., Maeda, Y. 1999. Atmospheric deposition of ^{35}S.
370   Journal of Radioanalytical and Nuclear Chemistry 239(3), 543-547.

371 Plummer, L.N., Busenberg, E., Bohlke, J.K., Nelms, D.L., Michel, R.L. 2001. Groundwater residence
372   times in Shenandoah National Park, Blue Ridge Mountains, Virginia, USA: a multi-tracer
373   approach. Chemical Geology 179, 93−111.

374 Schubert, M., Knöller, K., Tegen, I., Terzi, L. 2020a. Variability of Cosmogenic ^{35}S in Rain – Resulting
375   Implications for the Use of Radiosulfur as Natural Groundwater Residence Time Tracer. Water 12,
376   2953.

377 Schubert, M., Kopitz, J., Knöller K. 2020b. Low-sulphate water sample preparation for LSC detection
378   of ^{35}S avoiding sulphate precipitation. Journal of Environmental Radioactivity 213, 106153.

379 Schubert, M., Kopitz, J., Knöller, K. 2019. Improved approach for LSC detection of ^{35}S aiming at its
380   application as tracer for short groundwater residence times. Journal of Environmental
381   Radioactivity 208/209, 106022.

382 Shanley, J.B., Mayer, B., Mitchell, M.J., Michel, R.L., Bailey, S.W., Kendall, C. 2005. Tracing sources
383   of streamwater sulphate during snowmelt using S and O isotope ratios of sulphate and ^{35}S activity.
384   Biogeochemistry 76, 161-185.

385 Sueker, J.K., Turk, J.T., Michel, R.L. 1999. Use of cosmogenic ^{35}S for comparing ages of water from
386   three alpine/subalpine basins in the Colorado Front Range. Geomorphology 27, 61-74.

387 Tanaka, N., Turekian, K.K. 1991. Use of cosmogenic ^{35}S to determine the rates of removal of
388   atmospheric SO_2. Nature 352, 226-228.

389 Taylor, A., Keith-Roach, M.J., Iurian, A.R., Mabit, L., Blake, W.H. 2016. Temporal variability of
390   beryllium-7 fallout in southwest UK. Journal of Environmental Radioactivity 160, 80-86.

391   Turekian, K.K., Tanaka, N. 1992. The use of atmospheric cosmogenic ^{35}S and ^{7}Be in determining

392   depositional fluxes of SO_2. Geophysical Research Letters 19/17, 1767-1770.

393   Urióstegui, S.H., Bibby, R.K., Esser, B.K., Clark, J.F. 2015. Analytical Method for Measuring

394   Cosmogenic ^{35}S in Natural Waters. Analytical Chemistry 87, 6064-6070.

395   Urióstegui, S.H., Bibby, R.K., Esser, B.K., Clark, J.F. 2016. Quantifying groundwater travel time near

396   managed recharge operations using ^{35}S as an intrinsic tracer. Journal of Hydrology 543, 145-154.

397   Visser, A., Thaw, M., Deinhart, A., Bibby, R., Safeeq, M., Conklin, M., Esser, B., van der Velde, Y.

398   2019. Cosmogenic isotopes unravel the hydrochronology and water storage dynamics of the

399   Southern Sierra Critical Zone. Water Resources Research 55, 1429-1450.